Title

Exploring the Chemical Reactivity between Carbon Dioxide and Three Transition Metals (Au, Pt, and Re) at High-Pressure, High-Temperature Conditions

Journal

Inorganic Chemistry, 55(20)

ISSN

0020-1669

Authors

Santamaría-Pérez, David
McGuire, Chris
Makhluf, Adam
et al.

Publication Date

2016-10-17

DOI

10.1021/acs.inorgchem.6b01858

Peer reviewed

Inorganic Chemistry

Article

pubs.acs.org/IC

Exploring the Chemical Reactivity between Carbon Dioxide and Three Transition Metals (Au, Pt, and Re) at High-Pressure, High-Temperature Conditions

David Santamaría-Pérez,*[,†,‡] Chris McGuire,[†] Adam Makhluf,[†] Abby Kavner,[†] Raquel Chuliá-Jordán,[‡] Julio Pellicer-Porres,[‡] Domingo Martinez-García,[‡] Andrew Doran,[§] Martin Kunz,[§] Plácida Rodríguez-Hernández,[∥] and Alfonso Muñoz[∥]

[†]Earth, Planetary and Space Sciences Department, University of California Los Angeles, Los Angeles, California 951567, United States

[‡]Departamento de Física Aplicada-ICMUV, Universidad de Valencia, Valencia 46100, Spain

[§]Advanced Light Source, Lawrence Berkeley National Laboratory, Berkeley, California 94720, United States

[∥]Departamento de Física, Instituto Univ. de Materiales y Nanotecnología, Universidad de La Laguna, La Laguna, Tenerife, 38206 Spain

ABSTRACT: The role of carbon dioxide, CO_2, as oxidizing agent at high pressures and temperatures is evaluated by studying its chemical reactivity with three transition metals: Au, Pt, and Re. We report systematic X-ray diffraction measurements up to 48 GPa and 2400 K using synchrotron radiation and laser-heating diamond-anvil cells. No evidence of reaction was found in Au and Pt samples in this pressure−temperature range. In the Re + CO_2 system, however, a strongly−driven redox reaction occurs at P > 8 GPa and T > 1500 K, and orthorhombic β-ReO_2 is formed. This rhenium oxide phase is stable at least up to 48 GPa and 2400 K and was recovered at ambient conditions. Raman spectroscopy data confirm graphite as a reaction product. Ab-initio total-energy structural and compressibility data of the β-ReO_2 phase shows an excellent agreement with experiments, altogether accurately confirming CO_2 reduction $P-T$ conditions in the presence of rhenium metal and the β-ReO_2 equation of state.

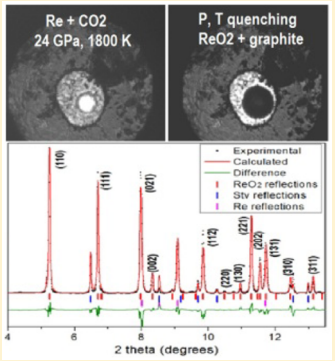

INTRODUCTION

Activation and reduction of CO_2 has been a subject of considerable investigation for many years because of (i) its abundance on Earth and (ii) the rapid increase of the CO_2 concentration in the atmosphere, intimately related with climate change.[1] In this context, the long-term CO_2 sequestration strategies are relevant. Heterogeneous reactions on clean transition metal surfaces have been considered in a number of studies,[2−10] and references therein, which helped better understanding of the energetics and reaction trajectories of metal/CO_2 interfaces. Thus, experiments and density-functional theory calculations suggested chemical mechanisms for CO_2 absorption, reactivity, and surface sensitivity on many metallic samples (Fe, Co, Ni, Pt, Cu, etc.).[3−9] It is proposed that CO_2 adsorption and subsequent dissociation on transition metals proceed through electron transfer from the metal to a CO_2 molecule to form an anion radical species, CO_2^-.[6] The change in polarization of the CO_2 species renders the carbon atom acidic, promoting absorption, in the form of carbonates, as well as dissociation.[10] It is also reported that the activation of CO_2 molecules is sensitive to the metal surface structure.[6−9] Segner et al., for instance, suggested from the results of scattering experiments on Pt(111)[9] that CO_2 dissociation is promoted preferentially at defect sites.

Oxidized carbon chemistry is of paramount importance in Earth sciences. CO_2 is often considered to exist in the deep Earth interior, its presence affecting the stability and physical properties of mantle phases. Different thermal and environmental conditions convert carbon dioxide into a variety of oxidized (carbonates) or reduced (diamond, graphite) carbon-bearing species.[11] The nature of these transformations is directly related to the bonding character and electron configuration in the C atom at high pressures and temperatures. The presence of potential reducing agents such as transition metals could provide constraints on the $P-T$ thermodynamic parameters for CO_2 carbon reduction and shed some light into the reaction mechanisms under different reduction−oxidation (redox) conditions.

High-density transition metals present a wide range of affinities for oxygen and could recreate a variety of redox environments. Thus, while gold oxides are thermodynamically unstable with respect to the elements, rhenium oxides are readily formed from oxidation of metallic Re at ambient pressure and relatively low temperatures. Note, for instance, that the Re-ReO_2 buffer is used in experimental petrology for controlling the oxygen fugacity.[12,13]

Received: August 26, 2016
Published: October 6, 2016

DOI: 10.1021/acs.inorgchem.6b01858
Inorg. Chem. 2016, 55, 10793−10799

Here, we report angle-dispersive synchrotron X-ray diffraction (XRD) data of the carbon dioxide + gold, platinum, or rhenium systems at pressures up to 48 GPa and temperatures up to 2400 K, using double-sided laser-heating in diamond-anvil cells (LHDACs). No evidence of reaction was found in Au and Pt samples in this pressure−temperature range. However, when Re metal was used as a laser absorber, XRD and Raman spectroscopy measurements confirm a CO_2 + Re → ReO_2 + C reaction associated with a pressure drop in the sample chamber. *Ab initio* total-energy calculations complement and describe in detail the elastic properties of β-ReO_2 rhenium oxide.

METHODS

To perform high-pressure high-temperature X-ray diffraction measurements, we used symmetric diamond-anvil cells (DACs). Au, Pt, and Re disks of 30 μm diameter and 4−12 μm thickness (coarse grains or pellets of precompressed powder) were placed at the center of a 80−110 μm diameter hole of tungsten gasket, preindented to a thickness of 40−50 μm. These metallic samples are good absorbers of the infrared radiation of the heating laser. Pure SiO_2 was used to thermally isolate the diamond anvils. High-purity CO_2 was loaded in the DAC at room temperature using the COMPRES gas loading apparatus. Ruby chips for pressure measurement were evenly distributed in the chamber. Pressures were measured before and after heating by the ruby fluorescence method.[14] The equations of state (EOS) of the metals were used as secondary pressure gauges.[15,16] A high-power diode-pumped fiber laser with wavelength of 1.07 μm was used to heat the metallic sample, with the flat-top laser intensity profile creating a 30 μm stable hotspot.[17] For temperature measurements, incandescent light was collected by aberration-free-reflecting objectives and detected with a high-resolution spectrometer. The temperature measurement system was calibrated with a tungsten filament light source with known intensity versus wavelength distribution. Planck's radiation function was then fitted to the collected spectrum assuming a constant emissivity value. Axial views down a typical DAC sample chamber configuration during laser heating and after thermal quench are shown in Figure 1.

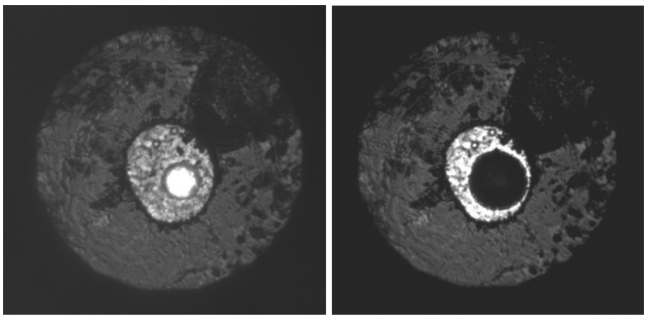

Figure 1. Images of the axial view down a typical diamond cell sample chamber configuration during laser heating (left) and after thermal quench (right). The 30 μm stable hotspot is shown. Two small ruby spheres are visible in the upper part of the transparent sample chamber.

Angle-dispersive X-ray diffraction measurements up to 48 GPa were carried out at two different synchrotron-based beamlines: GSECARS at the Advanced Photon Source and 12.2.2 at the Advanced Light Source. At GSECARS, incident X-rays had a wavelength of 0.3344 Å, the beam was focused to ~3 × 3 μm^2 spot, and diffraction patterns measured from 5 to 40 s were collected on a charge-coupled device (CCD) camera. At 12.2.2 at the ALS, incident X-rays with wavelengths of 0.4592 and 0.4959 Å were focused to 10 × 10 μm^2 and collected for 5−10 min on a MAR imaging plate. A precise calibration of the detector parameters was developed with a reference CeO_2 powder, and integration to conventional 2θ-intensity data was carried out with the Dioptas software.[18] The indexing and refinement of the powder patterns were performed using the FULLPROF[19] and POWDER-CELL[20] program packages.

Raman spectra were collected in the backscattering geometry using a 632.8 nm HeNe laser and a Jobin−Yvon TRH1000 spectrometer in combination with a Semrock 632.8 nm edge filter and a thermo-electric-cooled multichannel CCD detector. The spectra were calibrated using the plasma lines of the HeNe laser. The resolution and precision of the system are around 1 cm^{-1}. The laser power arriving to the DAC is less than 10 mW.

Ab initio total-energy calculations were performed within the framework of density-functional theory (DFT).[21] The Vienna Ab initio Simulation Package (VASP)[22] was used to carry out calculations with the pseudopotential method and the projector augmented wave (PAW) scheme, which replace the core electrons, make smoothed pseudovalence wave functions, and take into account the full nodal character of the all-electron charge density in the core region.[23] Exchange and correlation terms were introduced by means of the PBE functional within the solids prescription.[24] Alternatively, we have also used the GGA+U method to take into account the strong correlation between electrons in Re, on the basis of the Dudarev's method.[25] The Dudarev's approach dealt together with the onsite Coulomb interaction, U, and the exchange interaction J^H, defining an effective $U_{eff} = U - J^H$. In our study we choose U = 1 eV, a similar value to that used in other electronic-structure studies involving Re compounds.[26] The plane waves cutoff was set to 520 eV, and the convergence achieved in the total energy was less than 1 meV/atom.

RESULTS AND DISCUSSION

Our results show that no chemical reaction occurs in the sample chamber at high pressures and temperatures when gold and CO_2 were used. In this run, the sample was compressed to 24 GPa at room temperature, heated to 1700 K, quenched, further compressed to 46 GPa, heated to 2200 K, and finally quenched first in temperature and then in pressure, down to ambient conditions. After every heating run, we characterized the sample at high pressures and ambient temperatures, performing a two-dimensional XRD map of the pressure chamber traversing the laser-created hotspot. CO_2-I, -II, -III, -IV, and -V phases were observed at different P−T conditions, with the latter one being metastable during most of the downstroke pressure process. At 24 GPa and 1300 K, silica used as insulating material has fully transformed into stishovite, the thermodynamically stable phase of SiO_2 at these conditions. The X-ray diffraction pattern of the sample at 46 GPa after heating is shown in Figure 2. It illustrates the absence of chemical reaction and the quality of the XRD patterns at 46 GPa and ambient temperature. The high-pressure high-temperature (HP-HT) inertness of gold is in agreement with the ambient-pressure experimental evidence that gold is the least reactive metal toward atoms or molecules at the interface with a gas or a liquid.[27] Hammer and Norskov studied the dissociation of H_2 on several metal surfaces and, in the case of gold, reported both the highest energy barrier for dissociation and the least stable chemisorptions state. These two facts operate together to minimize the absorbate binding and subsequent reactivity of gold.[27] Liquid CO_2 + Au (e.g., at 24 GPa and 1700 K) is expected to behave similarly, with no reaction being observed in the studied P−T range.

In the case of the platinum + CO_2 system, several heating runs were carried out at pressures 8, 16, 24, 32, and 48 GPa up to 2000 K and no chemical reaction was observed. Partial decomposition of CO_2 forming diamond and probably ε-O_2 (Figure 3) was observed at relatively low temperatures (1700 K

DOI: 10.1021/acs.inorgchem.6b01858
Inorg. Chem. 2016, 55, 10793−10799

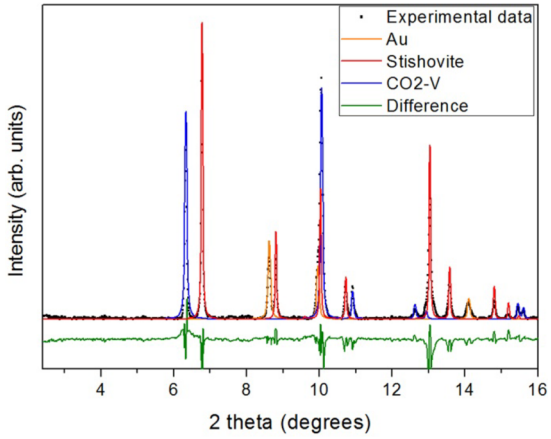

Figure 2. Rietveld refinement of the XRD pattern at 46 GPa and ambient temperature, after heating to 2100 K (λ = 0.3344 Å). Experimental data are depicted as scattered squares, and calculated XRD profiles of Au, SiO_2 stishovite, and CO_2–V are represented as orange, red, and blue lines, respectively. The full difference profile is represented as a green line.

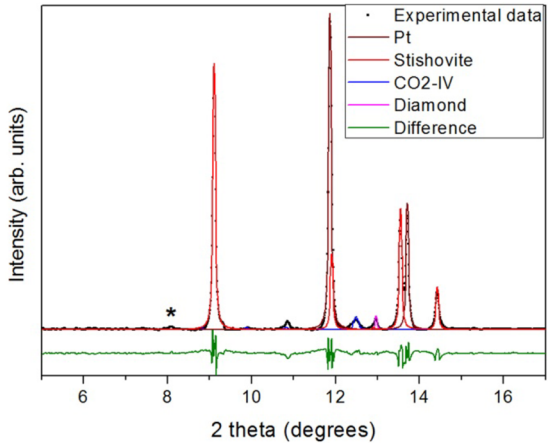

Figure 3. Rietveld refinement of the XRD pattern at 24 GPa and ambient temperature, after heating to 1700 K (λ = 0.4592 Å). Experimental data are depicted as scattered squares. Calculated XRD profiles of Pt, SiO_2 stishovite, CO_2-IV, and diamond are represented as wine, red, blue, and magenta lines, respectively. The full difference profile is represented as a dark green line. The peak at low angles marked with an asterisk could correspond to the reflection (0 0 1) of the ε-O_2 phase.

at 24 GPa). All the XRD patterns could be explained by the different CO_2 phases, from I to V, various SiO_2 polymorphs, high-quartz or -stishovite (depending on the pressure), Pt, diamond, and two low-intensity Bragg peaks, likely arising from ε-O_2. The observation of diamond diffraction features from partial CO_2 break down at pressures and temperatures well below those previously reported for this transformation[28] could have to do with the presence of platinum, a well-known catalyst, in the pressure chamber.

Three independent LHDAC runs were carried out in the Re + CO_2 system, covering the 8–48 GPa pressure and 295–2200 K temperature range. Two of these runs had silica as insulating material and followed P–T paths with several compressing and heating steps (see Figure 4, for instance). In the third one, only carbon dioxide and metallic rhenium were loaded in the DAC, which was then compressed up to 16 GPa and heated up.

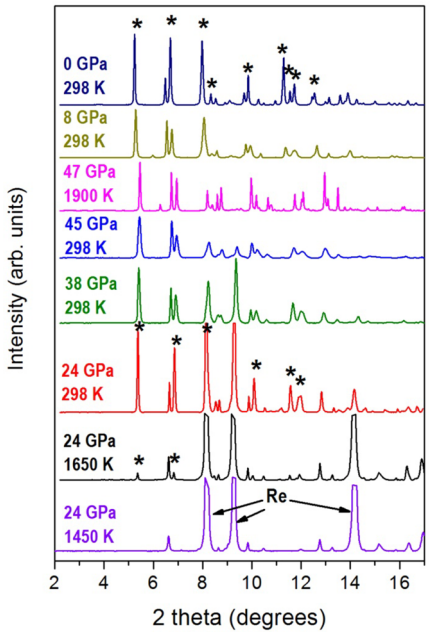

Figure 4. XRD data at several selected pressures and temperatures when Re was used as heater (λ = 0.3344 Å). The sample was first heated at 24 GPa, then compressed to 47 at room temperature, again heated at 47 GPa, and finally decompressed down to room pressure. Bragg peaks of β-ReO_2 are marked with asterisks only in the XRD patterns at 24 GPa and the quenched sample, but they can be clearly identified in the other XRD patterns. The rest of the peaks can be indexed as a combination of stishovite, CO_2-IV, and CO_2-V phases and rhenium metal.

Above 8 GPa and temperatures of 1500–1600 K, we observe a new phase that coexists with stishovite and is present up to 48 GPa (the sample was further compressed after temperature quenching) and also during the entire decompression process down to ambient conditions (see Figure 4).[29] A possible chemical reaction with silica was ruled out from our third experimental run, where the same new phase was observed.

A careful indexing of 16 diffraction peaks of the recovered sample suggests an orthorhombic structure with lattice parameters: a = 4.809(2), b = 5.640(7), and c = 4.599(2) Å, and a unit-cell volume of 124.75(12) Å^3. These unit-cell parameters are consistent with the *Pbcn* structure reported by Magneli[30] for β-ReO_2. Rietveld refinement of X-ray diffraction patterns in the 0–48 GPa pressure range shows that the Bragg peak intensities, systematic absences, and unit cell dimensions all show excellent agreement with those predicted for the *Pbcn* β-ReO_2 structure. Figure 5 illustrates the quality of the refinements. The inset of the figure shows the CCD raw diffraction image, which evidences that diffraction intensities mostly correspond to randomly oriented powder. Experimental and theoretical lattice parameters and atomic coordinates of this compound at room conditions are collected in Table I. No significant differences were found between the calculation with or without the U Hubbard term. Chemical reactivity and inertness of Re and Pt, respectively, at 8 < P < 48 GPa and 300 < T < 2200 K was additionally confirmed in a run where two independent samples of these metals were loaded in the same sample chamber.

Figure 4 shows a series of X-ray diffraction patterns from one of the Re-CO_2(-SiO_2) experiments at several selected pressures and temperatures. In this run, β-ReO_2 was formed at 24 GPa

DOI: 10.1021/acs.inorgchem.6b01858
Inorg. Chem. 2016, 55, 10793–10799

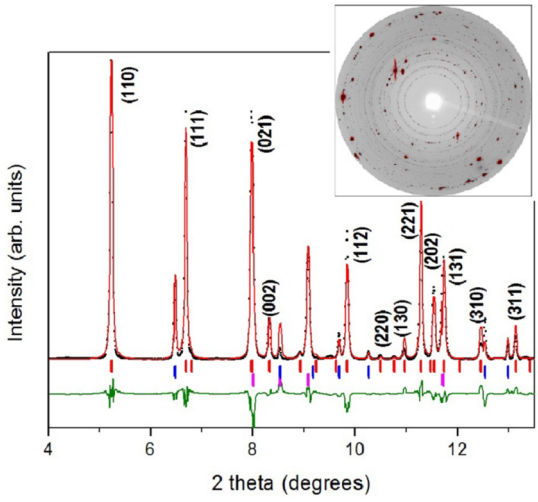

Figure 5. Rietveld refinement of the XRD pattern at ambient conditions, after heating to 2000 K and compressing to 48 GPa (λ = 0.3344 Å). Experimental data are depicted as scattered squares, and calculated and difference XRD profiles are represented as red and green lines, respectively. Bragg reflection positions of Re, SiO_2 stishovite, and β-ReO_2 phases are denoted as purple, blue, and red vertical ticks. The X-ray diffraction image is shown to illustrate the quality of the data.

Table I. Experimental and Calculated PBEsol Lattice Parameters, Volumes, and Fractional Coordinates of Orthorhombic *Pbcn* ReO_2 Recovered at Ambient Conditions

	XRD (This study)	Theoretical PBEsol (This study)	Theoretical PBEsol + *U* (This study)	XRD (ref 30)
a	4.8051(3)	4.8479	4.8386	4.8094(5)
b	5.6381(4)	5.6400	5.6655	5.6433(5)
c	4.6031(3)	4.5717	4.5782	4.6007(5)
V	124.71(7)	125.0	125.5	124.87
y_{Re}	0.113(1)	0.1072	0.1068	0.11
x_O	0.237(3)	0.2409	0.2413	0.25
y_O	0.362(2)	0.3599	0.3601	0.36
z_O	0.397(2)	0.4087	0.4093	0.375

and 1600 K. Under compression, typical peak broadening is observed in the X-ray patterns. From XRD data, we obtained the pressure dependence of the volume and lattice parameters of the orthorhombic rhenium oxide. The experimental and theoretical pressure−volume curves were analyzed using a third-order Birch−Murnaghan equation of state, obtaining the zero-pressure volume (V_0), the bulk modulus (B_0), and its pressure derivative (B'_0) collected in Table II. The fit of the EOS to our pressure−unit-cell volume data is shown in Figure 6 (top). The evolution for the unit-cell parameters of β-ReO_2 is shown in Figure 6 (bottom). Relative contractions for *a*, *b*, and *c* axes between room pressure and 45.3 GPa are 4.4, 2.8, and 3.8%, respectively, indicating that the compressibility of this oxide is slightly anisotropic. Experimental and theoretical compression data are in excellent agreement and support the identification of the observed phase. It is worth stressing the large incompressibility of this oxide ($B_0 \sim 300(20)$ GPa), which is higher than Al_2O_3 corundum ($B_0 \sim 252$ GPa) and comparable to SiO_2 stishovite ($B_0 \sim 291$ GPa).[31]

Table II. Experimental and Theoretical Zero-Pressure Volumes (V_0), Bulk Moduli (B_0), and Their Pressure Derivatives (B'_0) for β-ReO_2 Using a Birch−Murnaghan EOS

	V_0 (Å^3)	B_0 (GPa)	B'_0
Experimental	124.7(3)	277(24)	7.3(14)
Experimental 2	124.79 (fixed)	320(4)	4 (fixed)
Theoretical PBEsol	125.014(4)	306.2(3)	3.96(2)
Theor. PBEsol + U	125.49(1)	294.5(13)	3.88(10)
Theor. ref 39	120.915	321.8	4.24

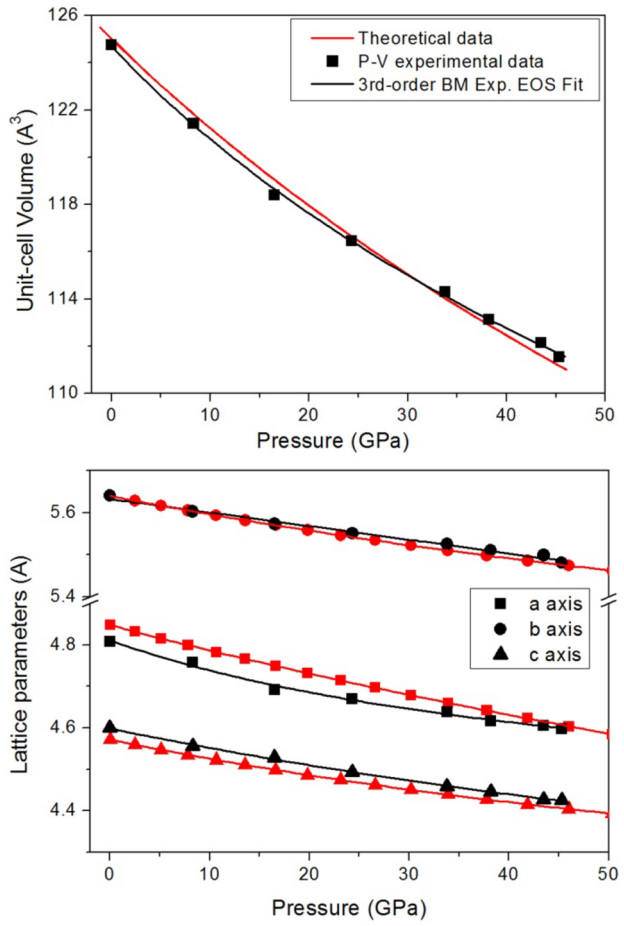

Figure 6. (Top) Pressure dependence of the unit-cell volume for orthorhombic *Pbcn*-β-ReO_2 under compression. Experimental and theoretical data are represented by black and red symbols, respectively. (Bottom) Evolution of the lattice parameters of β-ReO_2 with pressure according to our experimental (black symbols) and *ab initio* data (red symbols). Continuous lines represent guides to the eye.

Raman spectroscopic measurements on high-pressure high-temperature-quenched samples confirm the formation of the β-ReO_2 phase by a concurrent rhenium oxidation and carbon reduction process. Experimental Raman modes are in relative good agreement with the calculated ones (Figure 7 (top)). It is worthy to note that the metallic conductivity of this oxide, which will be discussed below, is the cause of a weak Raman activity. Raman spectra also show the existence of a broad band that corresponds to the vibrations within the graphene planes in graphite, often called the "G band". This band is centered at 1671 cm^{-1} for a pressure of 21 GPa (Figure 7 (bottom)).[32] Moreover, the strong diamond peak from the diamond anvil has a high-frequency shoulder that could correspond to the D

DOI: 10.1021/acs.inorgchem.6b01858
Inorg. Chem. 2016, 55, 10793−10799

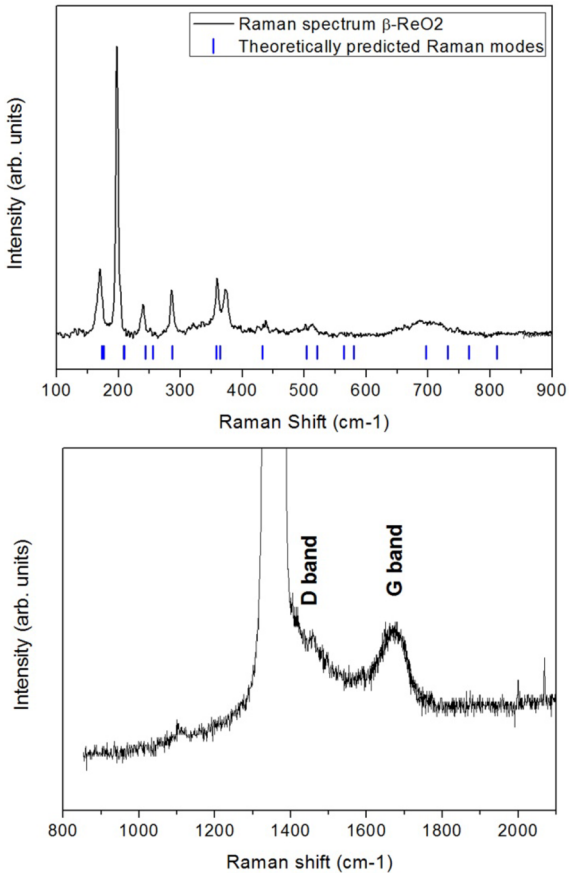

Figure 7. (Top) Ambient-conditions Raman scattering spectrum of β-ReO_2 recovered after compression and heating. Blue vertical marks correspond to theoretically predicted Raman modes. (Bottom) G Raman band characteristic of the vibrations within graphene planes in graphite from the spectrum at 21 GPa after heating. The most intense peak corresponds to crystalline diamond from the anvil, asymmetrically widened by stress conditions.

peak of disordered graphite. Therefore, Raman measurements support the hypothesis of a redox reaction where the carbon in CO_2 reduces to graphite and Re oxidizes to form β-ReO_2. No observation of graphite in our XRD experiments could be explained by either (i) the possible amorphous nature of this graphite product or (ii) the covering up of a high-Z scatterer like ReO_2.

The crystal structure of β-ReO_2, depicted in Figure 8, accounts for its large incompressibility. This oxide has a columbite-type (α-PbO_2) structure and consists of [ReO_6] octahedra sharing edges along the *c* axis and corners in the other two crystallographic directions. Every O atom in β-ReO_2 has three Re near neighbors that form a planar triangular [Re_3O] unit. This structure has been found as postrutile (and poststishovite) phases for TiO_2 (and SiO_2) oxides at high pressures.[33,34] In this regard, it is important to mention that two other ReO_2 polymorphs are reported in the literature: (i) A $P2_1/c$ monoclinic phase with a MoO_2-type structure[35] and (ii) a $P4_2/mnm$ tetragonal phase with a rutile-type structure.[36] These two phases share with orthorhombic β-ReO_2 the presence of edge-sharing [ReO_6] octahedra. In β-ReO_2, however, kinking of the chains allows further volume decrease of the unit-cell, i.e. a denser structure. Studies on some α-PbO_2 isomorphic oxides under compression suggest a possible phase transformation in β-ReO_2 to the monoclinic baddeleyite ZrO_2-type phase at

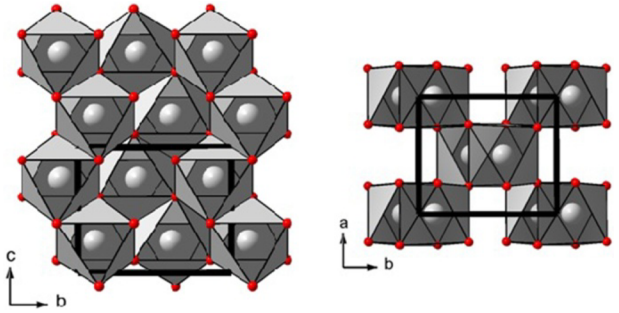

Figure 8. Structure of the β-ReO_2 phase. Light gray and red circles represent Re and O atoms, respectively. Recentered oxygen octahedra are shown. (Left) Projection on to the *bc* plane to illustrate the kinking of [ReO_6] chains. (Right) Projection on to the *ab* plane.

higher pressures,[33,37] but this transition was not experimentally observed below 48 GPa. According to our theoretical calculations, β-ReO_2 is metallic with antiferromagnetic ordering. The metallic behavior is related to the short Re−Re separation within the chains (2.62 Å at ambient conditions), which indicates a metal−metal bonding. Note that the Re−Re distance at ambient conditions in elemental rhenium is 2.73 Å. It has been suggested elsewhere[38] that the orthorhombic symmetry permits Re atoms bonding with two near Re neighbors to utilize all three t_{2g} orbitals in metallic bonding. A bond-order of about 1.5 was tentatively estimated.[38] No significant change in atomic coordinates occurs during compression, and the octahedral [ReO_6] arrangement is stable in the studied pressure range. According to experiments (calculations), the Re − O distances at room pressure in these octahedral units are 2 × 1.94 Å + 2 × 2.01 Å + 2 × 2.06 Å (2 × 1.98 Å + 2 × 2.00 Å).

CONCLUSIONS

In summary, carbon dioxide at high pressures and temperatures interacts differently with the transition metals considered in this study: Au, Pt, and Re. Gold is chemically inert, and no effect on liquid or solid CO_2 was observed. Platinum is also chemically inert in the studied $P-T$ range, but it seems to induce the CO_2 decomposition into its elements, diamond and ε-O_2, at gentler conditions than previously reported. Finally, rhenium oxidizes to form ReO_2 at pressures above 8 GPa and temperatures above 1500−1600 K and carbon of CO_2 reduces to graphite. This strong redox reaction gives rise to the orthorhombic β-ReO_2 polymorph, a metal oxide with unusually high bulk modulus (B_0 ∼ 300 GPa). Its structural and vibrational properties under compression have been studied by XRD and Raman spectroscopy measurements together with concurrent *ab initio* total-energy calculations.

AUTHOR INFORMATION

Corresponding Author

*E-mail: David.Santamaria@uv.es.

Author Contributions

D.S.P., C.McG., A.M., A.K., A.D., and M.K carried out in situ synchrotron-based X-ray diffraction experiments under high-pressure and high-temperature conditions. A.D. and M.K. also made in working order the BL 12.2.2 at ALS; D.S.P., D.M.G., and J.P.P. performed the Raman experiments; D.S.P. and R.C.J. analyzed the crystal structures and diffraction patterns; A.M. and P.R-H. conducted the DFT calculations; D.S.P. wrote the

DOI: 10.1021/acs.inorgchem.6b01858
Inorg. Chem. 2016, 55, 10793−10799

manuscript, but all authors discussed the experimental and theoretical results.

Funding

This work was supported by the Marie Curie Action PIOF-GA-2013-622439. Financial support from the Spanish Consolider Ingenio 2010 Program (Project No. CSD2007-00045), the Spanish government MEC under Grant No. MAT2013-46649-C4-1/3-P, and the Deep Carbon Observatory is also acknowledged. Supercomputer time has been provided by the Red Española de Supercomputación (RES) and the MALTA cluster. Portions of this work were performed at GeoSoilEnviroCARS (Sector 13), Advanced Photon Source (APS), and Argonne National Laboratory. GeoSoilEnviroCARS is supported by the National Science Foundation - Earth Sciences (EAR-1128799) and Department of Energy - GeoSciences (DE-FG02-94ER14466). This research used resources of the Advanced Photon Source, a U.S. Department of Energy (DOE) Office of Science User Facility operated for the DOE Office of Science by Argonne National Laboratory under Contract No. DE-AC02-06CH11357. Use of the COMPRES-GSECARS gas loading system was supported by COMPRES under NSF Cooperative Agreement EAR 11-57758. The Advanced Light Source is supported by the Director, Office of Science, Office of Basic Energy Sciences, of the U.S. Department of Energy under Contract No. DE-AC02-05CH11231. Use of the beamline 12.2.2 at the ALS is supported by COMPRES, the Consortium for Materials Properties Research in Earth Sciences under NSF Cooperative Agreement EAR 10-43050.

Notes

The authors declare no competing financial interest.

REFERENCES

(1) Overview of Greenhouse Gases. US Environmental Protection Agency: http://www.epa.gov/climatechange/ghgemissions/gases/co2.html.

(2) Glezakou, V. A.; Dang, L. X. Spontaneous Activation of CO_2 and Possible Corrosion Pathways on the Low-Index Iron Surface Fe(100). *J. Phys. Chem. C* **2009**, *113*, 3691−3696.

(3) Osaki, T.; Toshiaki, M. Kinetic Studies of CO_2 Dissociation on Supported Ni Catalysts. *React. Kinet. Catal. Lett.* **2005**, *87*, 149−156.

(4) Liu, C.; Cundari, T. R.; Wilson, A. K. CO_2 Reduction on Transition Metal (Fe, Co, Ni, and Cu) Surfaces: In Comparison with Homogeneous Catalysis. *J. Phys. Chem. C* **2012**, *116*, 5681−5688.

(5) de la Peña ÓShea, V. A.; Gonzalez, S.; Illas, F.; Fierro, J. L. G. Evidence for Spontaneous CO_2 Activation on Cobalt Surfaces. *Chem. Phys. Lett.* **2008**, *454*, 262−268.

(6) Solymosi, F. *J. Mol. Catal.* **1991**, *65*, 337.

(7) Bradford, M. C. J.; Vannice, M. A. *Catal. Rev.: Sci. Eng.* **1999**, *41*, 1.

(8) Wambach, J.; Freund, H. J. In *Carbon Dioxide Chemistry, Environmental Issues*; Paul, J., Pradier, C.-M., Eds.; Athenaeum Press: Cambridge, 1994; p 31.

(9) Segner, J.; Campbell, C. T.; Doyen, G.; Ertl, G. *Surf. Sci.* **1984**, *138*, 505.

(10) Markovits, A.; Fahmi, A.; Minot, C. *J. Mol. Struct.: THEOCHEM* **1996**, *371*, 219.

(11) Dasgupta, R. Ingassing, Storage, and Outgassing of Terrestrial Carbon through Geologic Time. *Rev. Mineral. Geochem.* **2013**, *75*, 183−229.

(12) Pownceby, M. I.; O'Neill, H. S. Thermodynamic Data from Redox Reactions at High Temperatures. IV. Calibration of the Re-ReO2 Oxygen Buffer from EMF and NiO + Ni-Pd Redox Sensor Measurements. *Contrib. Mineral. Petrol.* **1994**, *118*, 130−137.

(13) Masotta, M.; Keppler, H.; Chaudhari, A. Fluit-Melt Partitioning of Sulfur in Differentiated Arc Magmas and the Sulfur Yield of Explosive Volcanic Eruptions. *Geochim. Cosmochim. Acta* **2016**, *176*, 26−43.

(14) Mao, K. K.; Xu, J.; Bell, P. M. Calibration of the Ruby Pressure Gauge to 800-Kbar under Quasi-Hydrostatic Conditions. *J. Geophys. Res.* **1986**, *91*, 4673−4676.

(15) Dewaele, A.; Loubeyre, P.; Mezouar, M. Equations of State of Six Metals above 94 GPa. *Phys. Rev. B: Condens. Matter Mater. Phys.* **2004**, *70*, 094112.

(16) Jeanloz, R.; Godwal, B. K.; Meade, Ch. Static Strength and Equation of State of Rhenium at Ultra-High Pressures. *Nature* **1991**, *349*, 687−689.

(17) Prakapenka, V. B.; Kubo, A.; Kutnetsov, A.; Laskin, A.; Shkurikhin, O.; Dera, P.; Rivers, M. L.; Sutton, S. R. Advanced Flat Top Laser Heating System for High Pressure Research at GSECARS: Application to the Melting Behavior of Germanium. *High Pressure Res.* **2008**, *28*, 225−235.

(18) Prescher, C.; Prakapenka, V. B. DIOPTAS: A Program for Reduction of Two-Dimensional X-Ray Diffraction Data and Data Exploration. *High Pressure Res.* **2015**, *35*, 223−230.

(19) Rodriguez-Carvajal, J. Recent Advances in Magnetic-Structure Determination by Neutron Powder Diffraction. *Phys. B* **1993**, *192*, 55−69.

(20) Nolze, G.; Kraus, W. Powdercell 2.0 for Windows. *Powd. Diffract.* **1998**, *13*, 256−259.

(21) Hohenberg, P.; Kohn, W. Inhomogeneous Electron Gas. *Phys. Rev.* **1964**, *136*, 864−871.

(22) Kresse, G.; Hafner, J. Ab Initio molecular dynamics for liquids metals. *Phys. Rev. B: Condens. Matter Mater. Phys.* **1993**, *47*, 558−561.

(23) Blöchl, P. E. Projector Augmented-Wave Method. *Phys. Rev. B: Condens. Matter Mater. Phys.* **1994**, *50*, 17953−17979.

(24) Perdew, J. P.; Ruzsinszky, A.; Csonka, G. I.; Vydrov, O. A.; Scuseria, G. E.; Constantin, L. A.; Zhou, X. L.; Burke, K. Restoring the Density-Gradient Expansion for Exchange in Solids and Surfaces. *Phys. Rev. Lett.* **2008**, *100*, 136406.

(25) Dudarev, S. L.; Botton, G. A.; Savrasov, S. Y.; Humphreys, C. J.; Sutton, A. P. Electron-Energy-Loss Spectra and the Structural Stability of Nickel Oxide: An LSDA + U Study. *Phys. Rev. B: Condens. Matter Mater. Phys.* **1998**, *57*, 1505−1509.

(26) Rustad, J. R. Density functional calculations of the enthalpies of formation of rare-earth orthophosphates. *Am. Mineral.* **2012**, *97*, 791−799.

(27) Hammer, B.; Norskov, J. K. Why gold is the noblest of all the metals. *Nature* **1995**, *376*, 238−240.

(28) Tschauner, O.; Mao, H. K.; Hemley, R. J. New Transformations of CO_2 at High Pressures and Temperatures. *Phys. Rev. Lett.* **2001**, *87*, 075701.

(29) Santamaria-Perez, D.; McGuire, C.; Makhluf, A.; Kavner, A.; Chulia-Jordan, R.; Jorda, J. L.; Rey, F.; Pellicer-Porres, J.; Martinez-Garcia, D.; Rodriguez-Hernandez, P.; Muñoz, A. Strongly-driven Re + CO_2 Redox Reaction at High-Pressure High-Temperature Conditions. *Nature Commun.* **2016**, In Press.

(30) Magneli, A. Studies on Rhenium Oxides. *Acta Chem. Scand.* **1957**, *11*, 28−33.

(31) Léger, J. M.; Haines, J.; Schmidt, M.; Petitet, J. P.; Pereira, A. S.; da Jornada, J. A. H. Discovery of hardest known oxide. *Nature* **1996**, *383*, 401−401.

(32) Odake, S.; Zinin, P. V.; Hellebrand, E.; Prakapenka, V.; Liu, Y.; Hong, S.; Burgess, K.; Ming, L. C. Formation of the high pressure graphite and BC8 phases in a cold compression experiment by Raman scattering. *J. Raman Spectrosc.* **2013**, *44*, 1596−1602.

(33) Al-Khatatbeh, Y.; Lee, K. K. M.; Kiefer, B. High-Pressure Behavior of TiO_2 as Determined by Experiment and Theory. *Phys. Rev. B: Condens. Matter Mater. Phys.* **2009**, *79*, 134114.

(34) Murakami, M.; Hirose, K.; Ono, S.; Ohishi, Y. Stability of $CaCl_2$-type and α-PbO_2-type SiO_2 at High Pressure and Temperature Determined by in situ X-ray Measurements. *Geophys. Res. Lett.* **2003**, *30*, 1207.

(35) Ferreira, F. F.; Correa, H. P. S.; Orlando, M. T. D.; Passamai, J. L., Jr.; Orlando, C. G. P.; Cavalcante, I. P.; Garcia, F.; Tamura, E.;

DOI: 10.1021/acs.inorgchem.6b01858
Inorg. Chem. 2016, 55, 10793−10799

Martinez, L. G.; Rossi, J. L.; de Melo, F. C. L. Pressure Study of Monoclinic ReO_2 up to 1.2 GPa Using X-Ray Absortion Spectroscopy and X-Ray Diffraction. *J. Synchrotron Radiat.* **2009**, *16*, 48−56.
(36) Ivanovskii, A. L.; Chupakhina, T. I.; Zubkov, V. G.; Tyutyunnik, A. P.; Krasilnikov, V. N.; Bazuev, G. V.; Okatov, S. V.; Lichtenstein, A. I. Structure and Electronic Properties of New Rutile-Like Rhenium (IV) Dioxide ReO_2. *Phys. Lett. A* **2005**, *348*, 66−70.
(37) Errandonea, D.; Santamaria-Perez, D.; Bondarenko, T.; Khyzhun, O. New High-Pressure Phase of $HfTiO_4$ and $ZrTiO_4$ Ceramics. *Mater. Res. Bull.* **2010**, *45*, 1732−1735.
(38) Rogers, D. B.; Shannon, R. D.; Sleight, A. W.; Gillson, J. L. Crystal Chemistry of Metal Dioxides with Rutile-Related Structures. *Inorg. Chem.* **1969**, *8*, 841−849.
(39) Li, Y. L.; Zeng, Z. Structural, Elastic and Electronic Properties of ReO_2. *Phys. Lett. A* **2008**, *372*, 4086.

DOI: 10.1021/acs.inorgchem.6b01858
Inorg. Chem. 2016, 55, 10793−10799